Finite element method for epitaxial island growth

Frank Haußer*, Axel Voigt

Crystal Growth Group, Research Center caesar, Ludwig-Erhard-Allee 2, Bonn D-53175, Germany

Abstract

We present an adaptive finite element method for epitaxial island growth. The problem consists of an adatom diffusion equation on terraces of different height; boundary conditions on steps including the kinetic asymmetry in the adatom attachment and detachment; and the normal velocity law for the motion of the steps determined by a two-sided flux, together with diffusion of edge-adatoms along the steps. The problem is solved using two independent meshes: a two-dimensional mesh for the adatom diffusion and a one-dimensional mesh for the boundary evolution. Some applications demonstrating the influence of the Ehrlich–Schwoebel and inverse Ehrlich–Schwoebel barrier and the anisotropy are shown.
© 2004 Elsevier B.V. All rights reserved.

Keywords: A1. Anisotropy; A1. Edge diffusion; A1. Finite elements; A3. Adatom diffusion; A3. Ehrlich-Schwoebel effect; A3. Epitaxial growth

1. Introduction

Epitaxial growth is a modern technology of growing single crystals that inherit atomic structures from substrates. Almost defect-free, high-quality materials that have a wide range of device applications can be produced. Microscopic processes in epitaxial growth include the deposition of atoms or molecules, atom adsorption and desorption, adatom diffusion, adatom island nucleation, the attachment and detachment of adatoms to and from steps, and island coalescence, see Refs. [1,2].

We will consider a low-temperature regime, in which the island growth mode predominates. In a situation where islands are already nucleated and

grown to a specific size step edges serve as sinks of diffusion adatoms and mass currents of adatoms are established on the surface. In a typical situation in regard to such a growth mode, adatoms diffuse on a terrace and likely hit a step. In order to stick to the boundary from an upper terrace, an adatom must overcome a higher-energy barrier—the Ehrlich–Schwoebel barrier, see Refs. [3–5]. This asymmetry in attachment and detachment of adatoms to and from terrace boundaries has many important consequences: It induces an uphill current which in general destabilizes nominal surfaces (high symmetry surfaces) [3–5], but stabilizes vicinal surfaces (surfaces that are in the vicinity of high symmetry surfaces) with large slope, preventing step bunching [6]. However, such surfaces are unstable towards step meandering, and lead to the Bales–Zangwill morphological instability of atomic steps [7]. On the other hand step bunching observed on semiconductor surfaces

*Corresponding author.
  E-mail addresses: hausser@caesar.de (F. Haußer),
voigt@caesar.de (A. Voigt).

[8,9], requires a downhill current, which may be caused by an inverse Ehrlich–Schwoebel barrier— a barrier for adatoms arriving from the lower terrace. This mechanism destabilizes surfaces towards step bunching, but suppresses step meandering. These effects where recently studied both experimentally and theoretically in a step flow regime on vicinal Si(0 0 1) surfaces in Ref. [10]. In general, there is strong evidence of the influence of the Ehrlich–Schwoebel barrier on the surface morphology of a growing film, see e.g. Ref. [11].

There are various kinds of models for epitaxial growth of thin films that are distinguished by different scales in time and space. Among them, continuum models can describe film surface morphology and predict long time growth laws in terms of scaling. One class of continuum models are the Burton–Cabrera–Frank (BCF) type island dynamics models, cf. Refs. [12–14,2]. Such a model is essentially a free boundary problem that consists of a diffusion equation for the adatom density on terraces, boundary conditions for the moving steps, and a velocity law for the motion of the steps. This free boundary problem has the following distinguished features: First, terraces have different heights. Thus, the description of the growth is continuous in the lateral directions but discrete in the growth direction; second, the adatom flux to the terrace boundary is two sided, from both upper and lower terraces; and third, the normal velocity of the steps is determined by the two-sided flux and can include step-edge diffusion of edge-adatoms along the steps.

Recently in Refs. [15,16] a finite element framework was developed for such a class of island dynamics models. In this paper we shortly review this framework and apply it to study anisotropic effects and the influence of the Ehrlich–Schwoebel and inverse Ehrlich–Schwoebel barrier on growing epitaxial islands.

2. Problem description

We denote by $\Omega \subset \mathbb{R}^2$ the projected domain of the film surface and assume that Ω is independent of time t. Moreover $\Omega_0 = \Omega_0(t) \subset \Omega$ denotes the projected domain of the substrate or the exposed film surface with the smallest layer thickness and $\Omega_i = \Omega_i(t) \subset \Omega, i = 1, \ldots, N$, the projected domain of the terrace of height i at time t, respectively. Thus, $N + 1$ is the total number of layers that are exposed on the film surface. The corresponding steps are denoted by $\Gamma_i(t) = \overline{\Omega_i(t)} \cap \overline{\Omega_{i-1}(t)}, i = 1, \ldots, N$. Denote by $\rho_i = \rho_i(x, t)$ the adatom density on terrace $\Omega_i(t)$ $(i = 0, \ldots, N)$ at time t. The adatom diffusion on a terrace is described by the diffusion equation for the adatom density

$$\partial_t \rho_i - \nabla \cdot (D\nabla\rho_i) = F - \tau^{-1}\rho_i \quad \text{in } \Omega_i(t),$$
$$i = 0, \ldots, N, \tag{1}$$

where $D > 0$ is the surface diffusivity, $F > 0$ is the deposition flux rate, and $\tau^{-1} > 0$ is the desorption rate. Throughout the paper the unit of length will be the substrate lattice spacing a. Thus the adatom density ρ denotes the number of adatoms per adsorption site. We assume that the adatom density satisfies the following kinetic boundary conditions on the island boundary $\Gamma_i(t)$ for $i = 1, \ldots, N$

$$-D\nabla\rho_i \cdot \vec{n}_i - v_i\rho_i = k_+(\rho_i - \rho^*(1 + \mu\kappa_i)), \tag{2}$$

$$D\nabla\rho_{i-1} \cdot \vec{n}_i + v_i\rho_{i-1} = k_-(\rho_{i-1} - \rho^*(1 + \mu\kappa_i)), \tag{3}$$

$\vec{n}_i$ and κ_i are the unit normal pointing from the upper to the lower terrace and the curvature of the boundary $\Gamma_i(t)$, respectively; v_i is the normal velocity of the step $\Gamma_i(t)$ with the convention that $v_i > 0$ if the movement of $\Gamma_i(t)$ is in the direction of $\vec{n}_i$; k_+ and k_- are the kinetic attachment rates from the upper and lower terrace to the boundary $\Gamma_i(t)$, respectively; ρ^* is a positive constant denoting the thermodynamic equilibrium density at straight steps and μ depending on the normal direction of the boundary $\Gamma_i(t)$ being proportional to the stiffness of the boundary $\Gamma_i(t)$. If γ denotes the orientation-dependent step free energy divided by $k_B T$, then μ is given by $\mu(\theta) = \gamma(\theta) + \gamma_{\theta\theta}(\theta)$, with θ the angle of the outer normal with the x-axis. With this notation $0 < k_+ < k_-$ models the Ehrlich–Schwoebel effect, whereas $0 < k_- < k_+$ models the inverse Ehrlich–Schwoebel effect. If $k_+, k_- \to \infty$, Eqs. (2) and (3) pass into the thermodynamic boundary condition

$$\rho_i = \rho_{i-1} = \rho^*(1 + \mu\kappa_i).$$

A numerical scheme for this case was introduced in Ref. [16]. For the motion of the steps, we assume the following law for the normal velocity v_i of the island boundary $\Gamma_i(t)$

$$v_i = - D\nabla\rho_i \cdot \vec{n}_i - v_i\rho_i + D\nabla\rho_{i-1}\cdot\vec{n}_i + v_i\rho_{i-1} + \partial_s(v\partial_s(\mu\kappa_i)), \qquad (4)$$

where v is a positive function denoting the (orientation-dependent) mobility of the edge diffusion, and ∂_s denotes the tangential derivative along the steps. The last term in Eq. (4) represents step edge diffusion of edge-adatoms along the steps.

3. Discretization

We shortly review the weak formulation and finite element discretization as introduced in Refs. [15,16]. A first-order implicit scheme in time is used. In each time step: (i) we update the discrete step boundaries by solving a geometric partial differential equation based on the adatom densities and the discrete step boundaries from the previous time step; (ii) we solve the diffusion equation to update the adatom densities using the adatom densities from the previous time step and the computed discrete representation of the steps.

3.1. Boundary evolution

Using the boundary conditions Eqs. (2) and (3) at $\Gamma_i(t)$ in the velocity formula Eq. (4) leads to the geometric PDE

$$v_i = \gamma_i + \beta\mu\kappa_i + \partial_s(v\partial_s(\mu\kappa_i)), \qquad (5)$$

with $\gamma_i = k_+(\rho_i - \rho^*) + k_-(\rho_{i-1} - \rho^*)$ and $\beta = (k_+ + k_-)\rho^*$. This equation can be interpreted as an equation for anisotropic (one-dimensional) "surface" diffusion with lower-order terms. A variational formulation and discretization using parametric finite elements is obtained as follows (see Refs. [15,16]). Introducing the position vector $\vec{x}_i$, the curvature vector $\vec{\kappa}_i$, and the velocity vector $\vec{v}_i$, a system of equations for $\vec{\kappa}_i$, κ_i, v_i, and $\vec{v}_i$ can be derived from Eq. (5). Using the geometric expression $\vec{\kappa}_i = -\partial_{ss}\vec{x}_i$, the velocity law Eq. (5), and the relations between the vector valued and scalar

quantities $\kappa_i = \vec{\kappa}_i \cdot \vec{n}_i$ and $\vec{v}_i = v_i\vec{n}_i$, we obtain

$$\vec{\kappa}_i = -\partial_{ss}(\vec{x}_i), \qquad (6)$$

$$\kappa_i = \vec{\kappa}_i \cdot \vec{n}_i, \qquad (7)$$

$$v_i = \gamma_i - \beta\mu\kappa_i + \partial_s(v\partial_s(\mu\kappa_i)), \qquad (8)$$

$$\vec{v}_i = v_i\vec{n}_i. \qquad (9)$$

Considering discrete time steps Δt, the boundary at time $t + \Delta t$ is represented in terms of the boundary at time t by updating the position vector $\vec{x}_i \leftarrow \vec{x}_i + \Delta t\vec{v}_i$. Plugging the updated position vector into Eq. (6) and multiplying Eqs. (6)–(9) with test functions ψ and $\vec{\psi}$ leads to the following weak formulation:

$$\int_{\Gamma_i}\vec{\kappa}_i\vec{\psi} - \Delta t\int_{\Gamma_i}\partial_s\vec{v}_i \cdot \partial_s\vec{\psi} = \int_{\Gamma_i}\partial_s\vec{x}_i \cdot \partial_s\vec{\psi},$$

$$\int_{\Gamma_i}\kappa_i\psi - \int_{\Gamma_i}\vec{\kappa}_i \cdot \vec{n}_i\psi = 0,$$

$$\int_{\Gamma_i}v_i\psi + \int_{\Gamma_i}v\partial_s(\mu\kappa_i)\partial_s\psi + \int_{\Gamma_i}\beta\mu\kappa_i\psi = \int_{\Gamma_i}\gamma_i\psi,$$

$$\int_{\Gamma_i}\vec{v}_i\vec{\psi} - \int_{\Gamma_i}v_i\vec{n}_i\vec{\psi} = 0.$$

The system is now discretized using parametric finite elements. Note that in the above formulation, the adatom densities ρ_i and ρ_{i-1} on the upper and lower terraces, respectively, are needed only for computing γ_i. Solving the resulting linear system on each boundary yields the new boundary. These new boundaries, together with their curvatures will enter in the next time-step for the adatom diffusion.

3.2. Adatom diffusion

Multiplying Eq. (1) by a test function ϕ and integration by parts leads to

$$\int_{\Omega_i}\partial_t\rho_i\phi + \int_{\Omega_i}D\nabla\rho_i \cdot \nabla\phi + \int_{\Gamma_{i+1}(t)}D\nabla\rho_i \cdot \vec{n}_{i+1}\phi - \int_{\Gamma_i(t)}D\nabla\rho_i \cdot \vec{n}_i\phi = \int_{\Omega_i}F\phi - \int_{\Omega_i}\tau^{-1}\rho_i\phi.$$

For each i this equation is extended to the whole time-independent domain Ω by setting $\rho_i, D_i, F_i, \tau_i^{-1} = 0$ outside of Ω_i. Taking account of the distributional time-derivatives of ρ_i at the

steps, denoted by $\dot{\rho}_i$, and using the boundary conditions Eqs. (2) and (3), see Ref. [15] for details, we obtain

$$
\int_\Omega \dot{\rho}_i \phi + \int_\Omega D_i \nabla \rho_i \cdot \nabla \phi
$$
$$
+ \int_{\Gamma_{i+1}(t)} k_-(\rho_i - \rho^*(1 + \mu\kappa_{i+1}))\phi
$$
$$
+ \int_{\Gamma_i(t)} k_+(\rho_i - \rho^*(1 + \mu\kappa_i))\phi
$$
$$
= \int_\Omega F_i \phi + \int_\Omega \tau_i^{-1} \rho_i \phi. \tag{10}
$$

Notice that for the derivation of Eq. (10) the convective terms in the boundary conditions Eqs. (2) and (3) are essential. Since Eq. (10) is solved for each ρ_i on the whole domain, there are two degrees of freedom at each boundaries $\Gamma_k(t)$, namely ρ_k and ρ_{k-1}. In this way the discontinuity in the adatom density at the steps can be resolved. Eq. (10) is discretized using an implicit Euler discretization in time and linear finite elements in space. An adaptive strategy is used in order to refine the numerical mesh close to the step edges. For details we refer to Ref. [15].

4. Numerical simulation

Growing circular island as a numerical test: Consider a single, circular island $\Omega_1(t)$ of radius $R(t)$ at time t that is growing on a concentric circular substrate with radius R_Ω. Using polar coordinates (r, θ) with the origin at the center of the circular island, the radially symmetric solution

of the quasi-stationary diffusion equation is given by (see Ref. [17])

$$
\rho_0(r, t) = \frac{F}{4D}(R(t)^2 - r^2) + \frac{FR_\Omega^2}{2D}\ln\left(\frac{r}{R(t)}\right)
$$
$$
+ \rho^*\left(1 + \frac{\mu}{R(t)}\right) + \frac{F}{2k_-}\left(\frac{R_\Omega^2}{R(t)} - R(t)\right),
$$
$$
\rho_1(r, t) = \frac{F}{4D}(R(t)^2 - r^2) + \rho^*\left(1 + \frac{\mu}{R(t)}\right) + \frac{FR(t)}{2k_+}.
$$

The circular boundary evolves like $R(t)^2 = FR_\Omega^2 t + R(0)^2$. Since $F/D \ll 1$, the quasi-stationary solution is supposed to be a good approximation, and serves as a benchmark for the numerical simulation. Fig. 1 shows the cross-section of the computed adatom density under isotropic conditions at various times for the three cases

$$
0 < k_+ < k_- < \infty, \quad 0 < k_+ = k_- < \infty \quad \text{and}
$$
$$
0 < k_- < k_+ < \infty.
$$

The initial radius of the island is $R(0) = 3$ (in units of lattice spacing a) growing on a substrate of radius $R_\Omega = 10$ with parameters $D = 10^5$, $F = 1$, $\rho^* = 10^{-4}$, $\mu = 0.1$, $v = 0.1$ and $k_\pm = 10^3$ or 10^4.

The influence of k_+ and k_- on the jump of ρ at step-edges is clearly observed. In Fig. 2 the numerical solution, which remains rotational symmetric, is compared with the analytical solution. The relative max-error is less than 2% and partly results from the initial condition $\rho_i^0 = \rho^*$ used in the simulation. Also note, that at time $t = 0.4$ the areas of the substrate and of the island are equal, which in the case of $k_+ = k_-$ leads to a continuous adatom density at the step-edge.
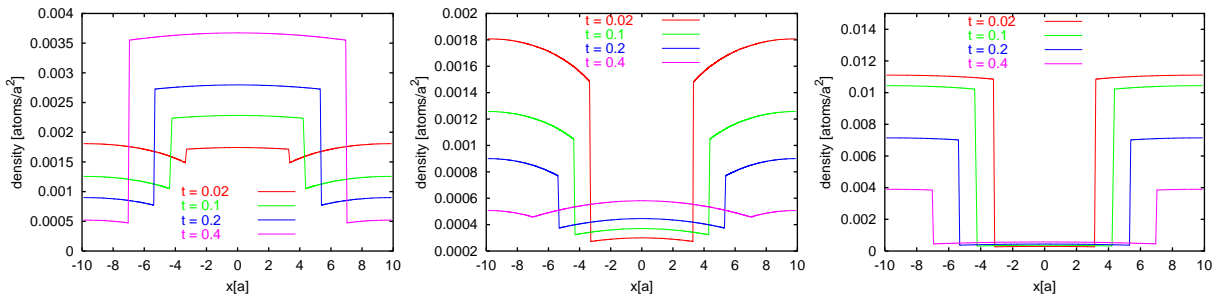

Fig. 1. Cross-sections of computed adatom densities: (left) $k_+ = 10^3$, $k_- = 10^4$; (middle) $k_+ = k_- = 10^4$; (right) $k_- = 10^3$, $k_+ = 10^4$.
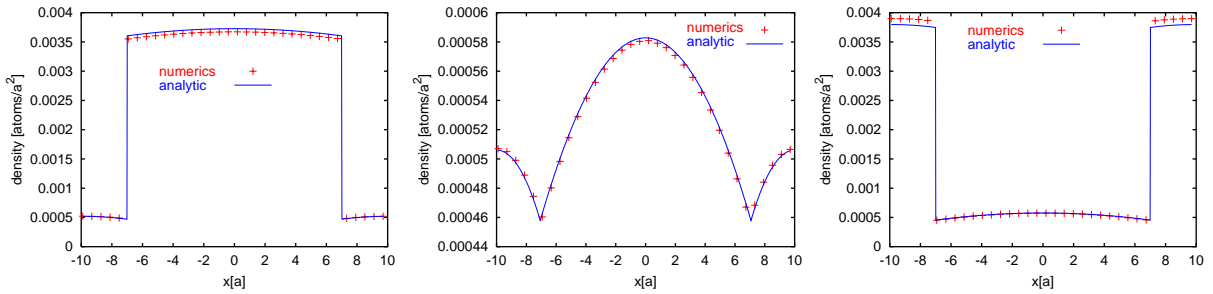
Fig. 2. Numerical and analytical solution at $t = 0.4$: (left) $k_+ = 10^3$, $k_- = 10^4$; (middle) $k_+ = k_- = 10^4$; (right) $k_- = 10^3$, $k_+ = 10^4$.
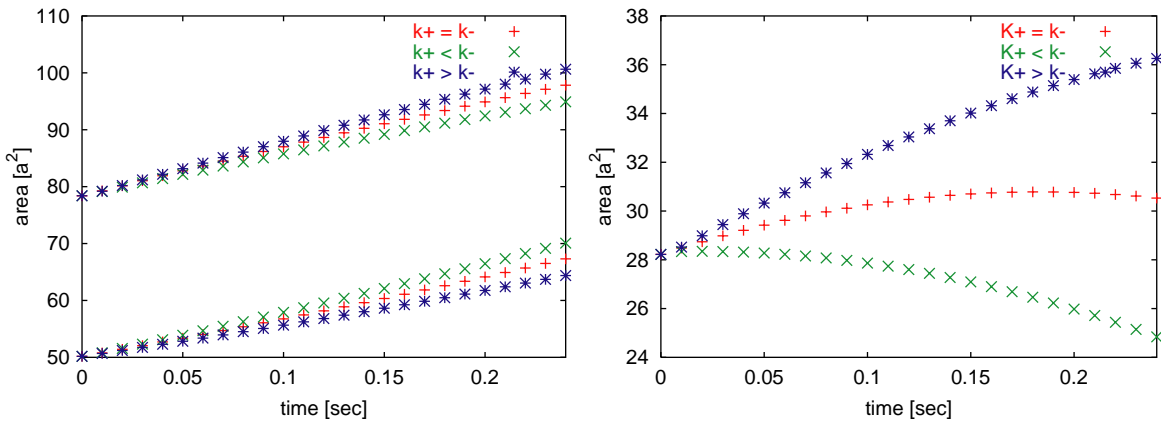

Fig. 3. (left) Island growth rates, (right) growth rate of intermediate terrace.

Dependency of growth rate on k_+ and k_-: The effect of the Ehrlich–Schwoebel and inverse Ehrlich–Schwoebel barrier is now analysed by simulating the evolution of two concentric islands with radii $R_1(0) = 5$ and $R_2(0) = 4$ sitting on top of each other on a circular domain of radius $R_0 = 7$.

Both islands grow, but the growth rate highly depends on the values of k_+ and k_-. Fig. 3 (left) shows the growth rate of both islands. The Ehrlich–Schwoebel barrier forces the adatoms to be incorporated at step-edges mainly from the lower terrace, which leads to an enlarged growth rate for the upper island but a reduced growth rate for the lower island. On the other hand the inverse Ehrlich–Schwoebel barrier forces the adatoms to be incorporated at step-edges mainly from the

upper terrace. This leads to a reduced growth rate for the upper island but an enlarged growth rate for the lower island. Thus the area growth rate of the intermediate terrace is reduced if $k_+ < k_-$ (Ehrlich–Schwoebel barrier) and enlarged if $k_+ > k_-$ (inverse Ehrlich–Schwoebel barrier), as seen in Fig. 3 (right).

Anisotropic growth: The final example shows the evolution of the two islands in the same setting as above but now including anisotropy. Thus we consider the step stiffness μ to be angle dependent and given by $\mu(\theta) = 1.0 - 0.8\cos(3\theta)$. Fig. 4 shows the adatom density at $t = 0.1$ and the adaptively refined two-dimensional mesh. The "triangular" shape as well as the jump at step-edges can clearly be observed. The time evolution is depicted in Fig. 5 where the one-dimensional curves,
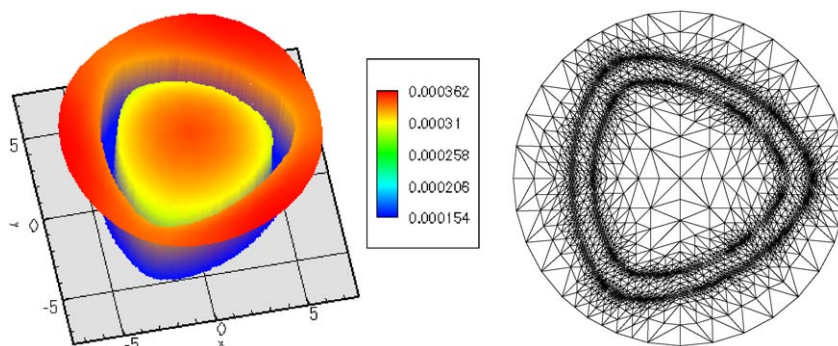
Fig. 4. Anisotropic growth: adatom density and adaptively refined mesh at $t = 0.1$.
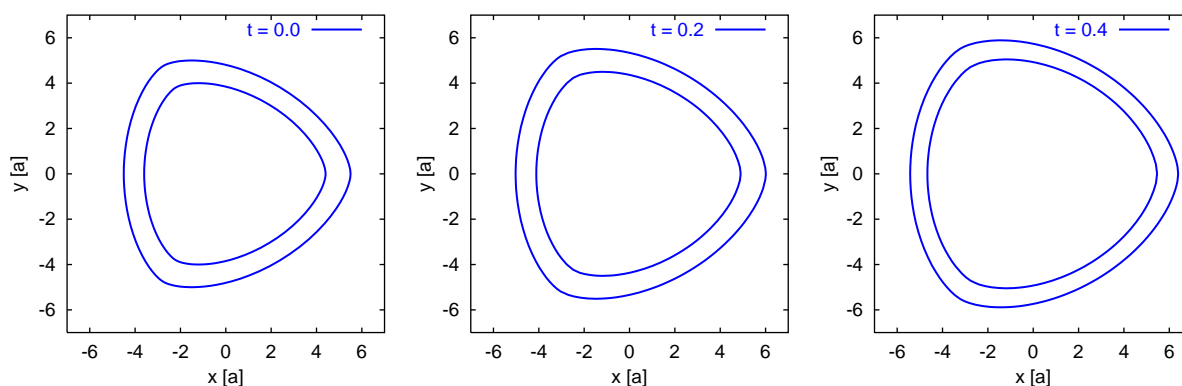

Fig. 5. Anisotropic growth: step edges of the two islands at various times.

corresponding to step-edges, are shown. It can be seen that the Wulffshape of the islands is nicely conserved during growth.

5. Conclusions

We have applied an adaptive finite element method to simulate island dynamics in epitaxial growth, taking account of anisotropies, attachment–detachment kinetics and diffusion of edge-adatoms along step-edge. After testing on analytic solutions, the method was applied to study the influence of an Ehrlich–Schwoebel and inverse Ehrlich–Schwoebel barrier on the evolution of two concentric islands. The algorithm described here is stable and fairly accurate and can be used for simulating island dynamics, in the absence of island nucleation and coalescence. The presented results are a first step towards the numerical simulations of the evolution of surface morphologies in the framework of step flow models, investigating the influence of the Ehrlich–Schwoebel effect.

References

[1] A.-L. Barabási, H.E. Stanley, Fractal Concepts in Surface Growth, Cambridge University Press, Cambridge, 1995.
[2] A. Pimpinelli, J. Villain, Physics of Crystal Growth, Cambridge University Press, Cambridge, 1998.
[3] G. Ehrlich, F.G. Hudda, J. Chem. Phys. 44 (1966) 1036.
[4] R.L. Schwoebel, J. Appl. Phys. 40 (1969) 614.
[5] R.L. Schwoebel, E.J. Shipsey, J. Appl. Phys. 37 (1966) 3682.
[6] J. Villain, J. Phys. I 1 (1991) 19.
[7] G.S. Bales, A. Zangwill, Phys. Rev. B 41 (9) (1990) 5500.
[8] C. Schelling, G. Springholz, F. Schäffler, Thin Solid Films 269 (2000) 1.

[9] P. Tejedor, F.E. Allegretti, P. Smilauer, B.A. Joyce, Surf. Sci. 407 (1–3) (1998) 82.

[10] J. Myslivecek, C. Schelling, F. Schäffler, G. Springholz, P. Smilauer, J. Krug, B. Voigtländer, Surf. Sci. 520 (2002) 193.

[11] M.G. Lagally, Z. Zhang, Nature 417 (2002) 907.

[12] W.K. Burton, N. Cabrera, F.C. Frank, Philos. Trans. R. Soc. London Ser. A 243 (866) (1951) 299.

[13] R. Ghez, S.S. Iyer, IBM J. Res. Dev. 32 (1988) 804.

[14] J. Krug, Physica A 318 (2002) 47.

[15] E. Bänsch, F. Haußer, O. Lakkis, B. Li, A. Voigt, J. Comput. Phys. 194 (2004) 409.

[16] E. Bänsch, F. Haußer, A. Voigt, Technical Report 36, Research Center Caesar, 2003.

[17] B. Li, A. Rätz, A. Voigt, Technical Report 50, SFB 611, Universität Bonn, 2002.